Measurement of hyperfine coupling constants in the $3d\ ^2D_j$ levels of ^{39}K, ^{40}K, and ^{41}K by polarization quantum-beat spectroscopy

A. Sieradzan, R. Stoleru, and Wo Yei
Physics Department, Central Michigan University, Mount Pleasant, Michigan 48859

M. D. Havey
Physics Department, Old Dominion University, Norfolk, Virginia 23529

(Received 21 October 1996)

Hyperfine quantum-beat spectroscopy has been utilized in a pump-probe configuration to measure magnetic dipole (A) and electric quadrupole (B) coupling constants in the $3d\ ^2D_{3/2}$ and $3d\ ^2D_{5/2}$ levels of three isotopes of potassium. For many of these levels, the largest hyperfine splitting is smaller than the natural width, and so a subnatural linewidth technique is required. In the experiments, the $3d$ levels are excited on the $4d\ ^2S_{1/2}\rightarrow 3d\ ^2D_j$ quadrupole transition with linearly polarized light. Time evolution of the alignment components in the d levels is probed by time-delayed resonant radiation on the $3d\ ^2D_j\rightarrow 9p\ ^2P_j$ transitions. Comparison of the excitation rate for two orthogonal relative polarization directions of the pump and probe laser at each delay time permits derivation of a linear polarization degree. This quantity contains beats at the various hyperfine frequencies in the d levels. Fitting the experimentally obtained time dependence to theoretical expressions allows extraction of the hyperfine coupling constants. For the $3d\ ^2D_{3/2}$ level of ^{40}K we obtain $A=0.96(4)$ MHz and $B=0.37(8)$ MHz, indicating a typical precision also obtained for the other levels and isotopes. [S1050-2947(97)04905-6]

PACS number(s): 32.10.Fn, 32.30.−r, 32.80.−t, 42.62.Fi

I. INTRODUCTION

Measurements of hyperfine structure of spectral lines have a long tradition in precision atomic spectroscopy. The measurements often serve as benchmarks for development of new techniques, and for refinement of atomic structure calculations [1–3]. The most precise measurements have been obtained for the hyperfine splitting of selected ground-level atoms, which serve as frequency standards. Determination of excited-level splittings has been much more difficult, due in part to the impeding effects of line-broadening mechanisms and the relative inefficiency of populating and detecting the signals. However, various laser-based techniques have led to impressive precision in many cases for excited levels of various atoms [1,3–17].

We recently refined and extended a technique, polarization quantum-beat spectroscopy, which leads to very precise determination of excited-level hyperfine structure [5,8,18]. The approach has been applied to measurement of the hyperfine structure of the $3p\ ^2P_{3/2}$ level in Na [8], the $4p\ ^2P_{3/2}$ level in ^{41}K [5], and the $5d\ ^2D_{3/2}$ and $5d\ ^2D_{5/2}$ levels in Cs [19]. In these experiments, the approach was seen to provide excellent agreement with other measurements, where comparisons could be made, but to yield results of considerably greater precision. The technique intrinsically obtains a subnatural linewidth resolution, which was particularly evident in the ^{41}K measurements, where the hyperfine levels are distributed over a width only slightly greater than the natural width of the transition of 6 MHz [20]. The approach is also robust, being free of major systematic errors, which allows for a very reliable modeling of the experimental signals.

In the hyperfine quantum-beat method [5,8], pulsed-laser excitation of an atomic level with polarized light produces a coherent superposition of amplitudes in the electronic magnetic states of the level. Excitation is presumed to take place on a time scale short compared to any hyperfine precession period. Modification of the superposition state via interaction with the nucleus through the hyperfine interaction redistributes the initially prepared amplitudes among other magnetic-substates. In the absence of dephasing due to collisions or external field fluctuations, the redistribution is reversible, leading to temporal oscillations in the amplitude associated with each magnetic level. The oscillations may be monitored by direct observation, in a selected direction, of the spontaneous decay as a function of time. Physically, this occurs because the angular distribution of the fluorescence depends on the m-state population distribution in the decaying level; or oscillations in the size of a signal generated by a polarized probe may be used. In this case, the anisotropy is monitored because the polarized probe measures the population in particular groups of m states, depending now on the state of polarization (and direction of propagation) of the probe light. Finally, an alternate view is that absorption of linearly polarized light generates alignment components in the excited level. These are related to the spatial configuration of the electronic charge distribution, which oscillates in time, and generates a time-dependent polarization and angular-dependent signal.

In this paper we report polarization quantum-beat measurements of the hyperfine structure in the $3d\ ^2D_j$ multiplet of the three stable isotopes of potassium ^{39}K, ^{40}K, and ^{41}K. The hyperfine structure in potassium is typically very small, and for several of the $3d$ multiplet components the largest hyperfine intervals are smaller than the natural width. Thus techniques other than those capable of subnatural width resolution are not readily applicable. Our previous measure-

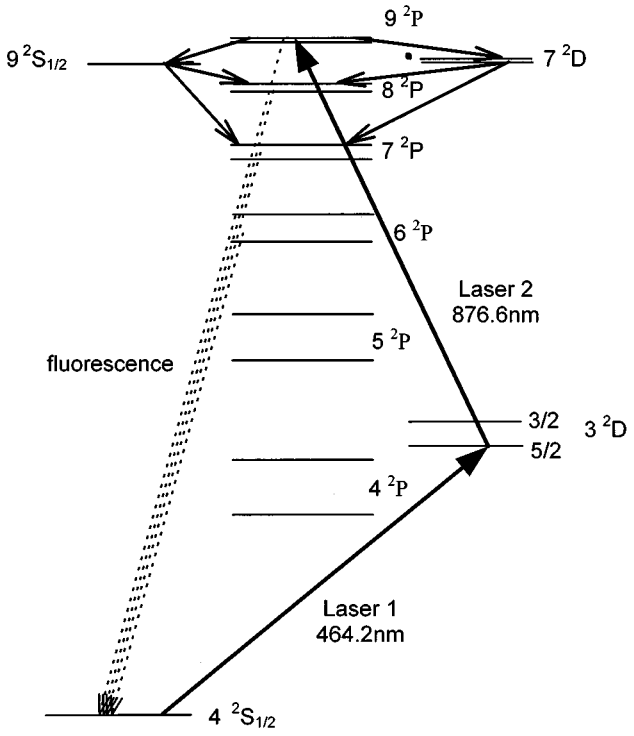

FIG. 1. Partial energy-level diagram for K, indicating excitation and fluorescence cascade pathways.

ments have clearly shown that such resolution is obtainable using polarization quantum-beat spectroscopy; in the present case, hyperfine coupling constants A and B were obtained to a few percent level. These measurements represent, to our knowledge, the first measurements of the hyperfine splitting in these levels, and also the where the hyperfine structure is buried within the natural width. We point out that the measurements are made particularly difficult for direct excitation and probing because of excitation via a very weak quadrupole transition, and because of lack of a convenient fluorescence pathway for detection of the excitation [20]. In the case of ^{40}K, the very low relative abundance ($\sim 10^{-4}$) of the isotope adds further difficulty [21].

In the following sections we first describe the experimental scheme and the hyperfine polarization quantum-beat-spectroscopy as it applies to the present case. This is followed by a detailed description of the experimental methodology and procedures. Analysis of the measurements and results is discussed, including the model used to extract hyperfine magnetic dipole and electric quadrupole coupling constants.

II. EXPERIMENTAL SCHEME

The basic excitation scheme of the experiment is shown in Fig. 1, which is a partial energy-level diagram for the potassium atom [20]. In the experiment, K atoms are brought to one of the $3d\ ^2D_j$ level components by linearly polarized radiation tuned to the quadrupole-allowed $4d\ ^2S_{1/2} \rightarrow 3d\ ^2D_j$ transitions around 464.2 nm. These transitions are quite weak, having an oscillator strength on the order of 10^{-6} [20]. Excitation of the $3d$ levels with linearly polarized radiation generates population and electronic multipole components [22] in the levels. For the $j=\frac{3}{2}$ fine-structure level, both population and second-rank (quadrupole) alignment components are generated, while in the $j=\frac{5}{2}$ level additional fourth-rank (hexadecapole) components exist. Since the hyperfine structure in the electronic levels is coherently excited by the relatively broadband excitation laser, the electronic multipole components in the laboratory frame have a time dependence depending on the various underlying hyperfine frequencies [22]. Atoms brought to the $3d\ ^2D_{3/2}$ or $3d\ ^2D_{5/2}$ level are probed after a variable time delay T relative to laser 1 by linearly polarized radiation tuned to one of the $3d\ ^2D_j \rightarrow 9p\ ^2P_{j'}$ fine-structure-resolved transitions around 876.6 nm. The stepwise excitation is monitored by detection of the ultraviolet direct and cascade fluorescence from the unresolved $np\ ^2P_{j'}$ levels ($n=6$, 7, 8, and 9) to the $4s\ ^2S_{1/2}$ ground level. The direction of linear polarization of laser 1 is adjustable to be collinear with or perpendicular to that of laser 2, generating signals $I_{\|}$ or $I_{\perp}$. These measurements are combined to form a linear polarization degree defined as $P_L=(I_{\|}-I_{\perp})/(I_{\|}+I_{\perp})$. By measurement of P_L at various selected delay times T, the time dependence of the electronic multipoles may be mapped, and the governing hyperfine frequencies then extracted by appropriate modeling.

As has been discussed in our previous papers [5,8,19], the sensitivity of the method is sufficient to obtain, in many cases, useful measurements for delay times as large as ten natural lifetimes of the state of interest. This, in turn, can result in ultimate resolution of approximately 0.1 times the natural width, depending on signal-to-noise ratio and systematic effects in the measurements. Subnatural width resolution is an essential feature in the success of the present measurements of the hyperfine structure in the $3d\ ^2D_j$ levels, for the largest contributing hyperfine interval [3,17] of several of the levels is on the order of or smaller than the natural width of about 4 MHz, which is determined primarily by the $3d\ ^2D_j \rightarrow 4p\ ^2P_j$ radiative decay channel.

A block diagram of the experimental apparatus is shown in Fig. 2. There it is seen that the laser 1 radiation was provided by a N_2-laser pumped dye laser having a typical energy of 20–100 μJ in a temporal pulse of about 10 ns. The device is configured as a grazing-incidence laser, providing a bandwidth of about 0.01 nm. This bandwidth permitted clear resolution of the individual fine-structure components, but completely overlapped the manifold of hyperfine levels. Two heavy-glass prisms were used to remove residual amplified spontaneous emission from the laser beam output. A crystal polarizer was used to define the linear polarization direction and purity, and a Pockels cell was employed to vary the polarization direction of the laser to be collinear or perpendicular to that of laser 2. The probe radiation from laser 2 was generated by a dye laser energized by the green second-harmonic radiation from a neodymium: yttrium aluminum garnet (Nd:YAG) laser. Laser 2 had a typical maximum power kept at a level below 70 kW in a pulse of around 8 ns in duration. For small delay times this was attenuated by 10^6–10^7 in order to maintain an acceptable photon counting rate of about 0.1 photon/laser shot. The laser bandwidth was typically 0.01 nm. As with laser 1, the polarization direction

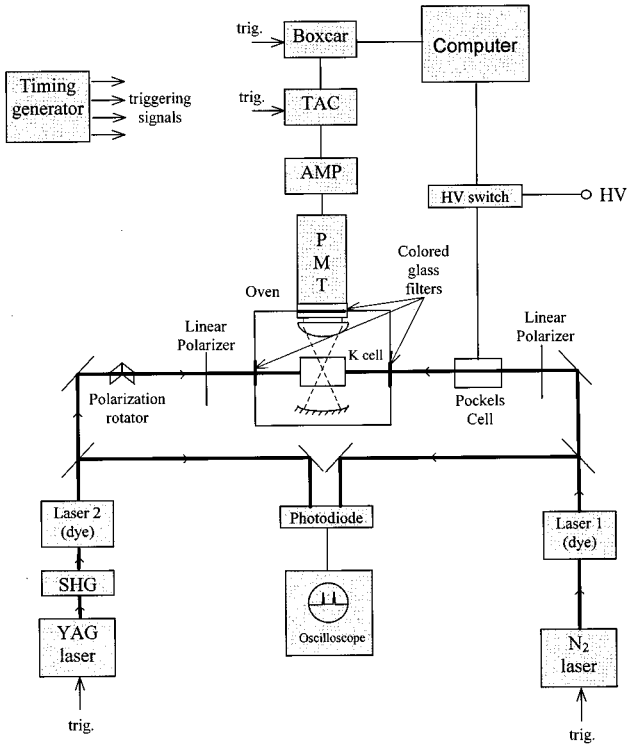

FIG. 2. Block diagram of the experimental apparatus.

was defined by a crystal linear polarizer. In addition, a polarization rotator was mounted in the laser 2 beam in order to vary the direction of the quantization axis associated with the final $np\ ^2P_j$ levels.

The two laser beams were counterpropagated through an oven-sample cell assembly mounted with flat windows to minimize variations in the transmitted intensity with polarization. The beams were overlapped in the central portion of the cell within a diameter of about 5 mm. The oven was maintained at a temperature of about 400 K, providing an estimated K density of 2.5×10^{12} cm^{-3}. Samples were prepared from isotopically enriched KCl salt by heating in the presence of Ca shavings, and then distillation under vacuum, of the released K metal, into the sample cells. These were then sealed off from the vacuum system and installed in the oven assembly. The base pressure in the cells at seal off was approximately 10^{-6} Torr. Note that isotopically enriched samples are necessary in the present case, for the naturally occurring abundances [21] are 93.3% (^{39}K), 6.7% (^{41}K), and 0.01% (^{40}K). In the present experiments, samples were of greater than 99% enrichment for ^{39}K and ^{41}K, and about 85% for ^{40}K.

The oven-cell assembly was constructed of nonmagnetic materials, and was heated with a bifilar heater which produced a negligible magnetic field outside the elements. The magnetic field of the earth was compensated for by Helmholtz coils which reduced the field in the oven region to less than 5 mG, as directly measured by a Hall-effect magnetometer. These precautions were taken to mitigate the potential effect of Zeeman beats superimposed on the hyperfine quantum beats of interest. Even for relatively short observation times, Zeeman beats can produce a weak modulation of the beat pattern which mimics a residual damping of the hyperfine beats.

Fluorescence signals were detected at right angles to the laser beams by a blue-only sensitive (<650 nm) photomultiplier (PMT) glass filter (4 mm of Corning type UG-11 glass) combination which permitted transmission of the desired ultraviolet signal light, but strongly rejected background light due to the laser beams. The signals were enhanced by collecting the light with a single condensing lens and by a convex mirror mounted opposite the detection arm. PMT signals were amplified and processed by a time-to-amplitude converter in combination with a boxcar averager. This combination permitted diagnostic measurements of the time-dependent fluorescence signals. These instruments were triggered by the timing generator so as to open the signal window for typically 2 μs following a delay of 500 ns relative to the probe laser. The 500-ns delay permitted additional suppression of signals due to laser scattering, and electronic pickup due to laser firing. Boxcar signal levels corresponding to single photon counting were accumulated for collinear and for perpendicular linear polarization directions of the pump and probe beams, yielding summed counting signals of $I_{\|}$ and $I_{\perp}$, respectively. Photon-counting levels were kept sufficiently low that dead time corrections were negligible. The counting signals were stored in a laboratory computer for later analysis, and for formation of a linear polarization degree P_L, as defined earlier. Switching of the polarization was accomplished by computer-controlled application of high voltage to the Pockels cell. To minimize distortion of the polarization measurements due to drifts in laser power and alignment, or other experimental conditions, the relative polarization direction was switched every five laser shots. A typical polarization measurement at a single time delay consisted of approximately 20 000–40 000 laser shots.

A critical feature of the experiment is measurement of the relative delay time between the two laser pulses. In earlier experiments [5,8,19], we used a direct measurement of the physical difference in travel distance between the pump-and-probe laser beams, which were pumped by a common source, to assess the delay time. This approach was essential, and convenient, in those cases, for a time base accuracy of better than 0.1 ns was required. In the present experiment the hyperfine beat frequencies are much smaller, and so a more convenient (because of the considerably longer delays used), although somewhat less accurate, approach was taken. The pump lasers were triggered by an external multioutput delay generator, which provided for a regulated delay between the two pulses. The pump-probe delay jitter of $\lesssim2$ ns associated with this approach is much less than the time resolution given by the laser pulse widths. A drift in the delay time was observed for longer runs, and was found to arise principally from small changes in the physical characteristics of the N_2 pump laser. These were primarily due to small drifts in the nitrogen gas pressure, lasing channel temperature, and drifts in the thyratron voltage. Drifts were assessed by directing a portion of each laser beam to a fast photodiode, the output of which was monitored by a 1-GHz oscilloscope. This approach was able to detect drifts larger than the jitter of about 2 ns. The occasional runs for which the drift was larger than this were not included in the data analysis.

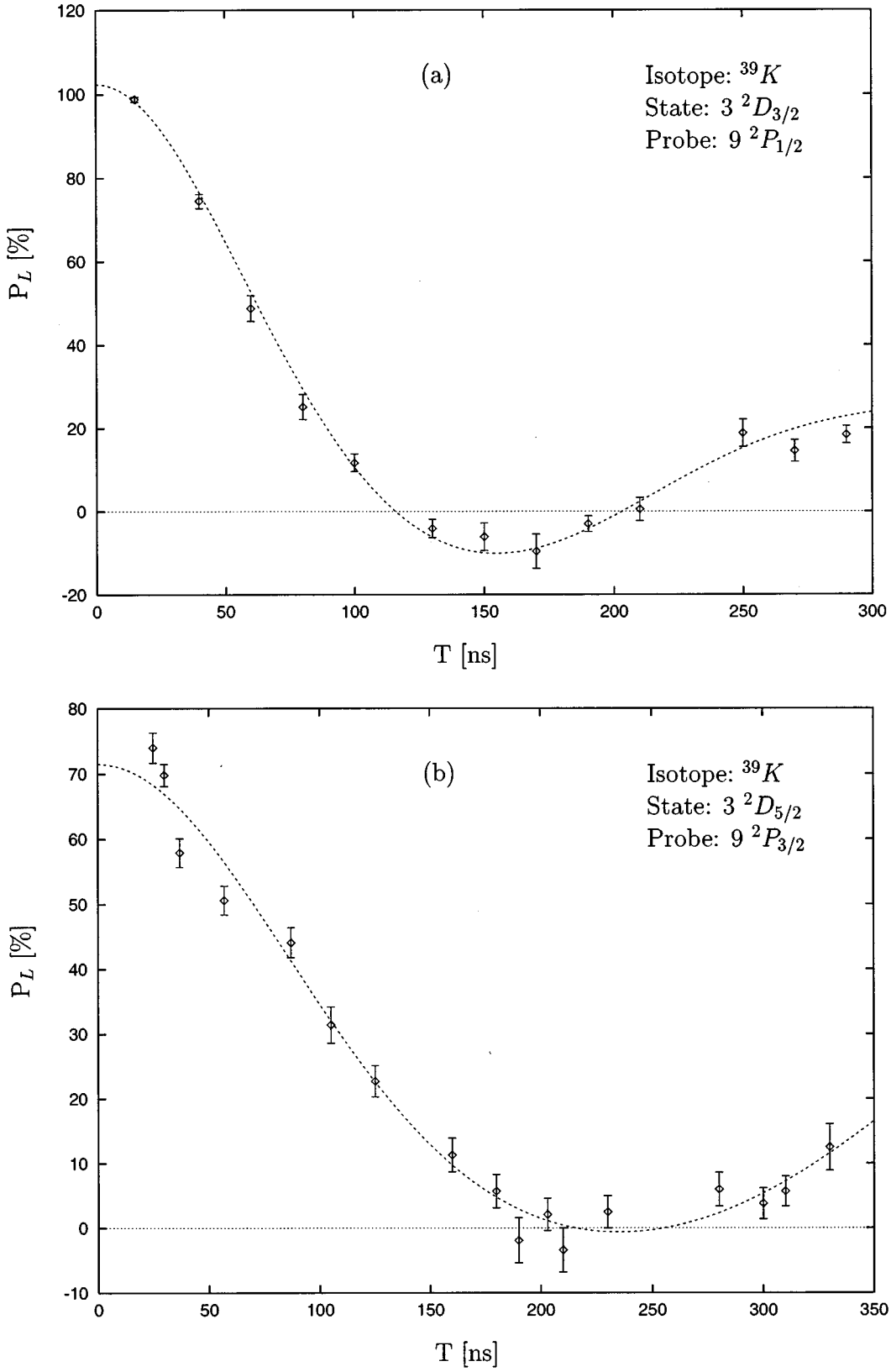

FIG. 3. Polarization quantum-beat data for ^{39}K. The dashed line represents the fit to the data. (a) $3d\ ^2D_{3/2} \rightarrow 9p\ ^2P_{1/2}$ transition. (b) $3d\ ^2D_{5/2} \rightarrow 9p\ ^2P_{3/2}$ transition.

III. ANALYSIS AND RESULTS

The main experimental quantity obtained from the measurements is a linear polarization degree P_L, defined in Sec. As discussed in earlier reports, polarization measurements may be readily made to very good precision, are normalized at each delay time, and display a high depth of modulation. These qualities provide some advantage over observation of

TABLE I. Experimental results for magnetic dipole (A) and electric quadrupole (B) hyperfine coupling constants for the $3d\ ^2D_{3/2}$ and $3d\ ^2D_{5/2}$ levels of ^{39}K, ^{40}K, and ^{41}K given in MHz. The amplitude fittting parameter is indicated as C, and is dimensionless. The cited errors on A and B represent *two* standard deviations.

Parameter	Level	^{39}K	^{40}K	^{41}K
A	$3d\ ^2D_{3/2}$	0.96(4)	1.07(2)	0.55(3)
B	$3d\ ^2D_{3/2}$	0.37(8)	0.4(1)	0.51(8)
C	$3d\ ^2D_{3/2}$	1.024(9)		0.939(13)
A	$3d\ ^2D_{5/2}$	0.62(4)	0.71(4)	0.40(2)
B	$3d\ ^2D_{5/2}$	<0.3	0.8(8)	<0.2
C	$3d\ ^2D_{5/2}$	0.95(3)		0.98(2)

quantum beats superimposed on a fluorescence or other decay curve, including simplification of the modeling of the data by elimination of the underlying decay curve. It is possible to eliminate or greatly reduce systematic effects associated with the polarization, so that direct comparison of the experimental and theoretical expressions may be made. In the present case, with colinear geometry and linearly polarized pump and probe beams, the theoretical formulas for the linear polarization degree for each multiplet transition are readily derived from the general results of Greene and Zare [23]:

$$P_L=\frac{3g}{4-g}, \quad {}^2D_{3/2}\rightarrow{}^2P_{1/2}, \tag{1}$$

$$P_L=\frac{-3g}{5+g}, \quad {}^2D_{3/2}\rightarrow{}^2P_{3/2}, \tag{2}$$

$$P_L=\frac{3g}{5-g}, \quad {}^2D_{5/2}\rightarrow{}^2P_{3/2}, \tag{3}$$

where the time-dependent alignment depolarization coefficient [22] $g(t)$ is given in general by

$$g(t)=\sum\sum\ [(2F+1)(2F'+1)/(2I+1)] \times W^2(JFJF';I,2)\cos(\omega_{FF'}t). \tag{4}$$

In this expression, F and F' are total angular momentum quantum numbers formed from I, the nuclear spin and J, the electronic angular momentum; $J=\frac{3}{2}$ and $\frac{5}{2}$. $W(\cdot)$ is a Racah coefficient and $\omega_{FF'}$ the hyperfine frequencies in the $3d\ ^2D_j$ levels. The summations run over all permitted values of F and F'. The nuclear spin values are $I=\frac{3}{2}$ for ^{39}K and ^{41}K, and $I=4$ for ^{40}K. Thus it is evident that the isotopic variations occur in $g(t)$, not in the general polarization expressions (1)–(3). Note that at $t=0$, $g=1$, and so these equations yield the purely electronic polarization depending only on the angular momentum quantum numbers in the initial and final levels. It is important to note that $g(t)$ is even upon sign reversal of the hyperfine coupling constants A and B, and thus only their relative signs may be determined.

Reliable modeling of the experimental data using the above expressions requires that systematic effects be either eliminated in the measurements or accounted for by extension of the model. In the present experiment, most systematic effects have been eliminated. The measured polarization at each delay did not measurably depend on the intensity of either laser, or on the density of K vapor in the cell. As discussed in the previous section, background magnetic fields were reduced to less than 5 mG, and so Zeeman beats were not observable on the time scale of the present experiments. Stray electric fields were estimated to be negligible for the experimental setup. The analyzing power of the polarimeter of ~ 0.999 was sufficient that the statistical uncertainty dominates any systematic effects associated with imperfect polarization.

Two effects can distort the measurements of the polarization. First, the finite temporal width of the pump-and-probe lasers can change the shape and amplitude of the beats present in $g(t)$. In the present case, this has been modeled by assuming rectangular laser pulses, which, when convoluted with $g(t)$ produce a phase shift and slight amplitude change for each hyperfine frequency component. Our previous measurements [5,8] have shown that a more elaborate modeling of the laser pulse shapes produces no significant improvement in results compared to using rectangular pulses, and so this model has been used in the present case. Second, a potentially serious physical effect is variation, with pump polarization, of the intensity of fluorescence detected by the PMT due to the different angular distribution of radiation emitted from the final np levels. Although the radiation emitted from $np\ ^2P_{1/2}$ levels is isotropic, that from $np\ ^2P_{3/2}$ levels is not. And even when probing is directly to the $9p\ ^2P_{1/2}$ level, cascade to lower $np\ ^2P_{3/2}$ levels, followed by hyperfine regeneration of electronic alignment [24], produces some anisotropy in the emitted intensity. Systematic tests were performed in ^{41}K to assess the extent of this effect. In one, final results (A and B) for excitation of each separate p-level fine-structure component were compared; these would have quite different angular distribution effects. In a second test, the direction of the probe laser relative to the detector was rotated by 90°. No difference in the quality of the fits to the data was found within experimental uncertainty for either arrangement, and so results for the hyperfine coupling constants were simply averaged. We presume that suppression of the angular distribution effect is due to the very large K-K collisional depolarization cross section ($\sim 10^4$ Å^2) [25] and quite long lifetimes of about 1.3 μs [26] for the final $9p$ levels, leading to collisional depolarization [27], and a resulting reduction of radiative anisotropy of the final levels. Note that as the collisional depolarization cross section should be much smaller in the $3d$ levels, and the lifetime of the levels is much shorter than the higher np levels, collisional reduction of the polarization is much reduced.

In general, hyperfine coupling constants [3] A and B were obtained by fitting the experimental data to expressions (1)–

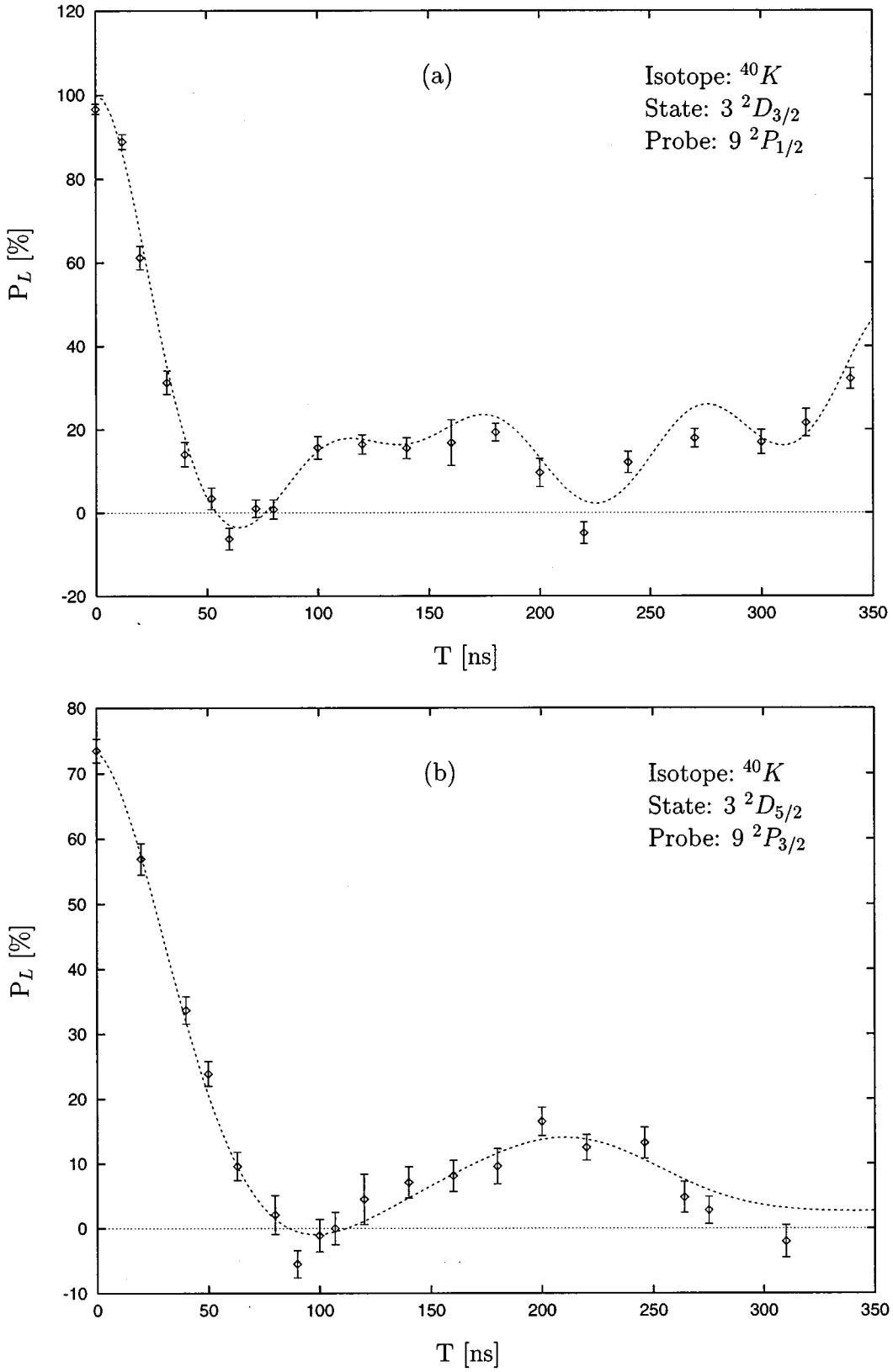

FIG. 4. Polarization quantum-beat data for ^{40}K. The dashed line represents the fit to the data. (a) $3d\ ^2D_{3/2} \rightarrow 9p\ ^2P_{1/2}$ transition. (b) $3d\ ^2D_{5/2} \rightarrow 9p\ ^2P_{3/2}$ transition.

(4), with the appropriate $g(t)$ as given below. A weighted least-squares fitting procedure was employed using as fitting parameters A, B, and an overall constant C inserted as a scale factor in the expressions for P_L. This factor was used to account for small depolarizing effects due to divergence of the laser beams, imperfect polarization of the lasers, and residual background signals. Each of these factors was found to be individually negligible. But the combined effect from

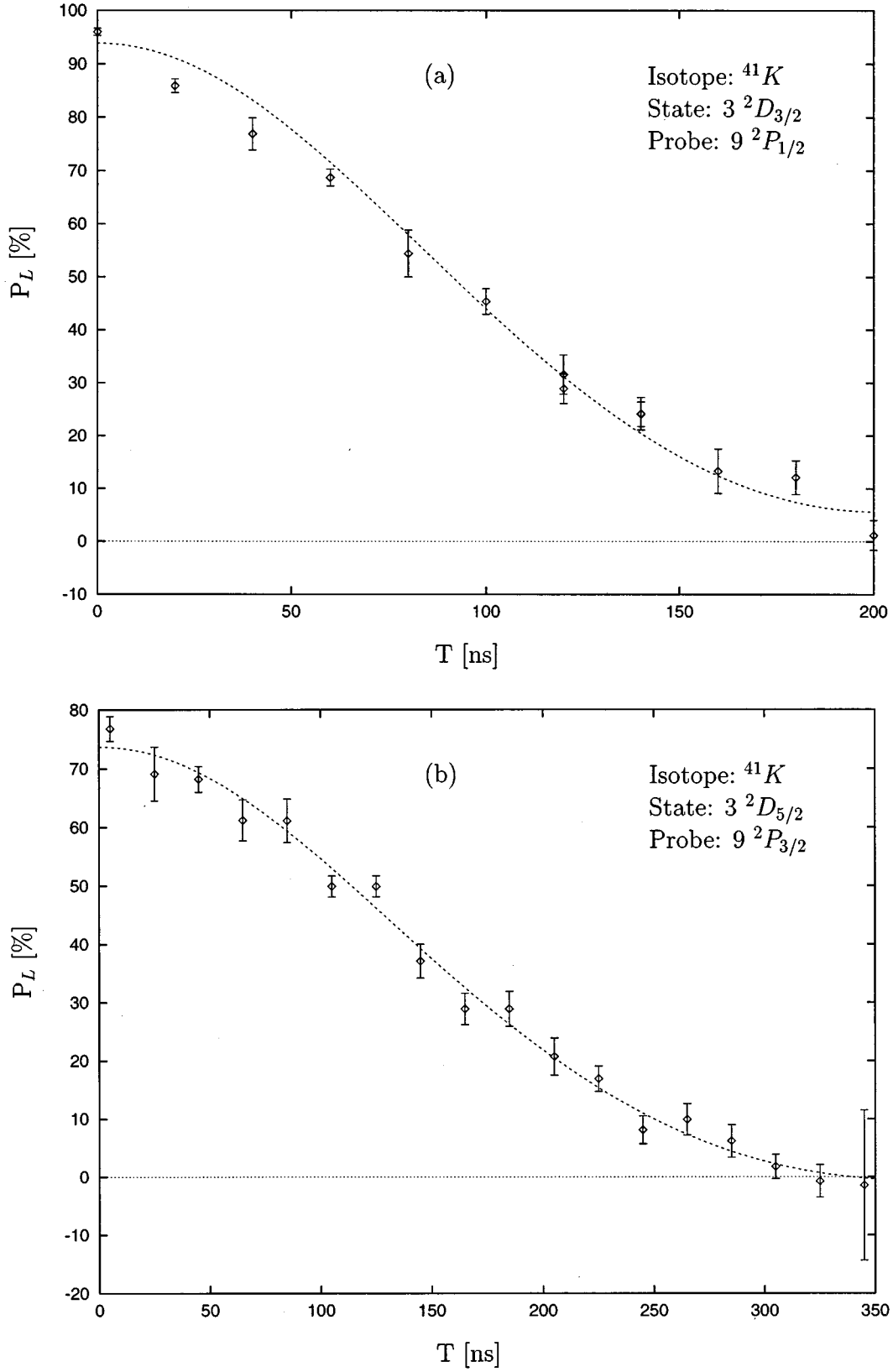

FIG. 5. Polarization quantum-beat data for ^{41}K. The dashed line represents the fit to the data. (a) $3d\ ^2D_{3/2} \rightarrow 9p\ ^2P_{1/2}$ transition. (b) $3d\ ^2D_{5/2} \rightarrow 9p\ ^2P_{3/2}$ transition.

all sources could be as large as a few percent of the maxiIII. mum polarization. In fitting the data, a χ^2 minimum was searched for as a function of A, B, and C. For each isotope and $3d$ multiplet component a clear minimum was found, yielding values for the fitting parameters. As no correlation in the errors was found, a one-standard deviation error was defined as the boundary of the χ^2+1 points for each parameter.

A. Results for ^{39}K

The depolarization coefficient $g(t)$ for the $3d\ ^2D_{3/2}$ level in ^{39}K, which has $I=\frac{3}{2}$, is given by

$$g(t)=\tfrac{27}{100}+\tfrac{1}{8}\cos 2\pi(3A-2B)t+\tfrac{3}{20}\cos 2\pi(2A-B)t+\tfrac{21}{200}\cos 2\pi(5A)t+\tfrac{7}{20}\cos 2\pi(3A+B)t. \quad (5)$$

Similarly, for the $3d\ ^2D_{5/2}$ level,

$$g(t)=\tfrac{46\,447}{117\,600}+\tfrac{3}{20}\cos 2\pi(2A-4B/5)t+\tfrac{3}{100}\cos 2\pi(5A-5B/4)t+\tfrac{169}{840}\cos 2\pi(3A-9B/20)t+\tfrac{9}{392}\cos 2\pi(7A+7B/20)t+\tfrac{45}{224}\cos 2\pi(4A+4B/5)t. \quad (6)$$

These equations, in combination with Eqs. (1) and (3), are used to fit the ^{39}K time-dependent polarization. The results of the fit, along with the experimental data, are presented in Fig. 3. There it is seen that there is very good qualitative agreement between experimental results and the fit. Note that, at $t=0$, the polarization should be 100% and 75% for the $^2D_{3/2}$ and $^2D_{5/2}$ levels, respectively. However, because the pump-and-probe lasers each have a width on the order of 10 ns, the experimental polarization at $t=0$ should be somewhat smaller than those values. For this isotope, data were not taken at small enough delays to observe this effect, but the $t=0$ intercept of the fit agrees with the ideal theoretical values to within the uncertainty of the fit. The χ^2 minimum for each of these fits is typically in the range of 1–4 with three adjustable parameters. The origin of the reduced χ^2 values being larger than the ideal value of 1 is likely the isotopic impurity, preventing more ideal modeling of the data, and residual time base jitter, which is not incorporated into the model. For this reason we quote an error representing two statistical intervals.

Results for the hyperfine coupling constants are presented in Table I. Note that for all results presented in the table, the quoted error represents two standard deviations. The results are consistent with the upper limits for A and B established by Lam, Gupta, and Happer [17]. They are also, as expected, considerably larger than the hyperfine coupling constants which have been measured for the $6d$ multiplet [15]. To our knowledge, no other experimental information exists on the hyperfine structure in the $3d\ ^2D_j$ levels of ^{39}K. Finally, for the $3d\ ^2D_{5/2}$ level, only an upper limit on the size of B could be determined. As the expressions for $g(t)$ are even in the sign of the hyperfine splitting, the relative signs of A and B could not be determined. Thus the positive value for A in Table I is meant to represent the absolute value of the magnetic dipole coupling constant. For the $3d\ ^2D_{3/2}$ level, the relative signs of A and B are determined from the data.

B. Results for ^{40}K

The depolarization coefficient $g(t)$ for the $3d\ ^2D_{3/2}$ level in ^{40}K, which has $I=4$, is given by

$$g(t)=\tfrac{22\,327}{103\,950}+\tfrac{20}{189}\cos 2\pi(7A/2-11B/16)t+\tfrac{11}{54}\cos 2\pi(8A-13B/14)t+\tfrac{4}{135}\cos 2\pi(9A/2-27B/112)t+\tfrac{112}{675}\cos 2\pi(10A+25B/56)t+\tfrac{416}{14\,852}\cos 2\pi(11A/2+11B/16)t. \quad (7)$$

Similarly, for the $3d\ ^2D_{5/2}$ level,

$$g(t)=\tfrac{14\,741}{64\,350}+\tfrac{8}{147}\cos 2\pi(5A/2-33B/112)t+\tfrac{110}{1323}\cos 2\pi(6A-333B/560)t+\tfrac{11}{98}\cos 2\pi(8A-69B/140)t+\tfrac{128}{2695}\cos 2\pi(9A/2-27B/140)t+\tfrac{26}{275}\cos 2\pi(10A-15B/112)t+\tfrac{8}{55}\cos 2\pi(11A/2+33B/560)t+\tfrac{14}{297}\cos 2\pi(12A+153B/280)t+\tfrac{560}{3003}\cos 2\pi(13A/2+39B/80)t. \quad (8)$$

Fitting the data for ^{40}K was made more involved than for the other two isotopes, for the samples for ^{40}K were somewhat isotopically contaminated by ^{39}K and ^{41}K, the quoted isotopic purity was about 90%. To account for this, the signals were presumed to arise from a fraction f of ^{40}K and, as the fractional isotopic contamination was not known, equal amounts $(1-f)/2$ of the other two isotopes. As ^{39}K and ^{41}K have qualitatively similar hyperfine beat patterns which are each much more slowly varying than those for ^{40}K, this should not seriously distort the results. The fraction f was taken as a fitting parameter, and the best-fit value was $f=0.83(3)$, a somewhat lower fraction than the cited value of $f=0.9$. For the $3d\ ^2D_{5/2}$ level, it was necessary to include an exponential damping constant in the expression for the polarization; the resulting weak decay constant was $0.0041(5)\ \text{ns}^{-1}$. The reason for the altered procedure in this case was that the very small amount of total sample mass for this isotope in the cell was disappearing with time, presumably by reaction with the cell walls. Several heating and cooling cycles of the cell did not improve the situation, but the higher temperatures than normal occurring in the procedure presumably increased somewhat the background gas level (and resulting depolarization collision rate) in the sealed-off cell. In these fits, the amplitude parameter was taken as $C=1$.

Final fits to the polarization beats for ^{40}K are presented in Fig. 4, along with the model results obtained using Eqs. (1)–(6) [the $g(t)$ expressions for ^{41}K are identical to those for ^{39}K]. It is seen from the figure that the fitting is qualitatively excellent, with the $t=0$ limit being evidently obtained within the statistical errors, and with the general shape of the beat curve reproduced by the model. Hyperfine coupling constants obtained from the fit, along with the associated 2σ errors, are presented in Table I. No experimental data from other sources exists for comparison. Finally, as was the case for the $3d\ ^2D_{5/2}$ level in ^{39}K, the sign of A remains undetermined from our data.

C. Results for ^{41}K

The depolarization coefficients for this isotope are identical to those for ^{39}K given in Sec. III A. Data and the results of the fit are presented in Fig. 5, where again the modeling results are seen to agree well with the experimental data. Hyperfine coupling constants, obtained for ^{41}K from the fit, and the corresponding 2σ errors, are presented in Table I. Again, as for ^{39}K and ^{40}K, the sign of A for the $3d\ ^2D_{5/2}$ level is not determined from the data. Finally, as was the case for the other isotopes, no experimental data from other sources exists for comparison.

TABLE II. Results of systematic tests for effects of final-state interactions on magnetic dipole (A) and electric quadrupole (B) hyperfine coupling constants for the $3d\ ^2D_{3/2}$ level of ^{41}K, given in MHz. The cited errors on A and B represent *one* standard deviation. Horizontal or vertical refers to the direction of the probe polarization. Horizontal polarization points along the axis of the detector, while vertical is perpendicular to that.

Test	Final level	Probe polarization	A (MHz)	B (MHz)
1	$9p\ ^2P_{1/2}$	horizontal	0.559(74)	0.7(5)
2	$9p\ ^2P_{3/2}$	horizontal	0.534(35)	0.561(76)
3	$9p\ ^2P_{3/2}$	vertical	0.512(25)	0.552(71)
4	$9p\ ^2P_{1/2}$	vertical	0.569(17)	0.462(42)
5	$9p\ ^2P_{3/2}$	vertical	0.584(71)	0.3(9)

For this isotope and for the $3d\ ^2D_{3/2}$ level, systematic tests were performed in order to assess the size of possible effects associated with the angular distribution of the fluorescence signals from the final np levels (as discussed qualitatively in an earlier section). These were (1) excitation of the two different $9p$ fine-structure components as final levels, and (2) varying the probe linear polarization direction to be either in line with, or perpendicular to the direction from the interaction region to the signal detector. Either of these tests should reveal any effects associated with the angular distribution of radiation emitted from the final level. As the results summarized in Table II show, no significant variations of A and B with these conditions was observed. Thus we quote the average values in Table I for this isotope.

IV. SUMMARY

Hyperfine coupling constants have been determined for the $3d\ ^2D_{3/2}$ and $3d\ ^2D_{5/2}$ levels in ^{39}K, ^{40}K, and ^{41}K. For several of these levels, the extent of the hyperfine splitting is smaller than the natural width. However, by utilizing the subnatural linewidth resolution inherent in polarization quantum-beat spectroscopy, the hyperfine splitting has been determined to a few percent precision for each isotope. The measurements represent the first experimental determination of the hyperfine structure in these isotopes, and demonstrate the capability of the experimental method employed.

The polarization hyperfine quantum-beat method has now been applied to selected levels in Na, K, and Cs. Magnetic dipole coupling constants for the various studies range from about 0.5 MHz to nearly 50 MHz, covering a range of 10^3 in this coupling constant. The method can yield excellent precision over this range, and could generally be extended to both higher- and lower-frequency ranges. Depending on the lifetime of the level of interest, other techniques will often be more readily applicable for higher frequencies. However, for smaller hyperfine splittings where the natural width is on the order of or smaller than the splitting, the present approach is an excellent method for measurement, yielding reliable results for coupling constants as small as 0.1 times the natural width.

ACKNOWLEDGMENT

The financial support of the National Science Foundation for this research is greatly appreciated.

[1] S. Haroche, *High Resolution Laser Spectroscopy* (Springer, New York, 1976).
[2] I. Lindgren and J. Morrison, *Atomic Many Body Theory* (Springer, Berlin, 1982).
[3] E. Arimondo, M. Inguscio, and P. Violino, Rev. Mod. Phys. **49**, 31 (1977).
[4] W. Demtröder, *Laser Spectroscopy* (Springer-Verlag, Berlin, 1982).
[5] A. Sieradzan, P. Kulatunga, and M. Havey, Phys. Rev. A **52**, 4447 (1995).
[6] G. D. Stevens, Chun-Ho Iu, S. Williams, T. Bergeman, and H. Metcalf, Phys. Rev. A **51**, 2866 (1995).
[7] N. Ph. Georgiades, E. S. Polzik, and H. J. Kimble, Opt. Lett. **19**, 1474 (1994).
[8] Wo Yei, A. Sieradzan, and M. D. Havey, Phys. Rev. A **48**, 1909 (1993).
[9] W. A. van Wijngaarden, J. Li, and J. Koh, Phys. Rev. A **48**, 829 (1993).
[10] J. Sagle and W. A. van Wijngaarden, Can. J. Phys. **69**, 808 (1991).
[11] W. A. van Wijngaarden and J. Sagle, Phys. Rev. A **43**, 2171 (1991).
[12] M. Głodź and M. Kraińska-Miszczak, Phys. Lett. A **160**, 85 (1991).
[13] W. A. van Wijngaarden and J. Sagle, J. Phys. B **24**, 897 (1991).
[14] R. Alheit, X. Feng, G. Z. Li, R. Schreiner, and G. Werth, J. Mod. Opt. **39**, 411 (1992).
[15] M. Głodź and M. Kraińska-Miszczak, J. Phys. B **18**, 1515 (1985).
[16] Carol E. Tanner and Carl Wieman, Phys. Rev. A **38**, 1616 (1988).
[17] L. K. Lam, R. Gupta, and W. Happer, Phys. Rev. A **21**, 1225 (1980).
[18] T. W. Ducas, M. G. Littman, and M. L. Zimmerman, Phys. Rev. Lett. **35**, 1752 (1975).
[19] W. Yei, M. D. Havey, A. Sieradzan, and E. Cerasuolo (unpublished).
[20] A. A. Radzig and B. M. Smirnov, *Reference Data on Atoms, Molecules, and Ions* (Springer-Verlag, Berlin, 1985).
[21] *CRC Handbook of Chemistry and Physics*, 62nd ed., edited by R. C. Weast and M. J. Astle (CRC, Boca Raton, FL, 1981).
[22] K. Blum, *Density Matrix Theory and Application* (Plenum, New York, 1981).
[23] C. H. Greene and R. N. Zare, Ann. Rev. Phys. Chem. **33**, 119 (1982).
[24] W. Happer, Rev. Mod. Phys. **44**, 169 (1972).
[25] T. F. Gallagher, *Rydberg Atoms* (Cambridge University Press, Cambridge, 1994).
[26] C. E. Theodosiou, Phys. Rev. A **30**, 2881 (1984).
[27] A. Gallagher, Phys. Rev. **157**, 68 (1967).